RSC Advances

ROYAL SOCIETY OF CHEMISTRY

www.rsc.org/advances

Journal Name

RSCPublishing

ARTICLE

Pd-loaded In_2O_3 nanowire-like network synthesized by CNTs templates for enhancing NO_2 sensing performance

Cite this: DOI: 10.1039/xoxxoooooox

Received ooth January 2012,
Accepted ooth January 2012

DOI: 10.1039/xoxxoooooox

www.rsc.org/

Mingqi. Huang [a], Zhenduo. Cui [a], Xianjin. Yang [a, b], Shengli. Zhu [a, b], Zhaoyang. Li [a, b], Yanqin. Liang [a,b*]

Pd-loaded In_2O_3 nanowire (NW)-like networks were synthesized via electroless plating using carbon nanotubes (CNTs) as templates, followed by oxidation and removal of the CNTs at 550 ℃. Palladium (Pd) was introduced to activate the surface of CNTs for subsequent plating. Owing calcination, Pd was loaded onto In_2O_3. The as-synthesized Pd-loaded In_2O_3 replicated the structure of the CNTs, forming a porous NW-like network with a very large specific surface area. Furthermore, the NO_2 gas sensing properties of the Pd-loaded In_2O_3 NW-like network, porous Pd-In_2O_3, and the porous unloaded-In_2O_3 were investigated. The results demonstrated that the Pd-In_2O_3 NW-like network exhibits superior sensitivity with a short response/recovery time, and it demonstrates a significant response when exposed to NO_2 at concentrations as low as 5 ppm at a temperature of 110 ℃. The synergy of electric and chemical effects has been proposed with the experimental results to explain gas sensing enhancement.

Introduction

Nitrogen dioxide (NO_2), as one of the major constituents of photochemical smog, is harmful to the environment and can also induce health problems. In order to detect and control NO_2, it is crucial to develop sensors with a low detection limit, low operating temperature and rapid response/recovery time. Gas sensors are very useful for many applications such as detection of toxic and deleterious gases, pollution abatement, public safety, and process control. There is an urgent demand for the development of high quality gas sensitive materials.[1-4] Indium oxide (In_2O_3), as a typical n-type semiconductor with a direct band gap of 3.55–3.75 eV, could potentially be used to detecting H_2S, CO, C_2H_5OH and NO_2 because of its high electrical conductivity, abundant defects and autocatalysis.[5-7] In recent years, In_2O_3 has been widely studied as a NO_2 gas sensor. Although the maximum response has been substantially improved, the response/recovery time is generally too long. Furthermore, the gas sensing mechanism is still unclear and further studies are required.

It is acknowledge that the properties of sensors significantly depend on their morphology and structure. In order to improve the sensitivity and shorten the response/recovery time, In_2O_3 has been designed and fabricated with various morphologies including nanoparticles,[8] nanowires,[9] nanotubes,[10] nanorods,[11] nanobelts,[12] and hollow spheres[13]. In consideration of the current investigations on the above nanomaterials, the quasi-1D nanomaterials (including nanotubes, nanowires, and nanobelts) would be expected to be the most promising structures for sensors because of their high surface to volume ratio and porous structure for gas diffusion.[14-17].

Until now, quasi-1D In_2O_3 has been prepared using several methods, such as sol–gel chemistry, electrospinning,[18-20] and the solid template method. The template method is commonly used to synthesize quasi-1D metal oxide. Carbon nanotubes (CNTs) are ideal templates in order to synthesize quasi-1D metal oxide because of their excellent acid and alkali resistance. Moreover, they can be removed at high temperatures. In early studies, Ning Du et al[21] prepared porous In_2O_3 nanotubes with polyelectrolytes using layer-by-layer assembly/deposition on CNTs, followed by calcination. Zhang[22] developed a novel strategy for the synthesis of CeO_2 nanotubes. This was performed by coating the CNTs with a continuous CeO_2 nanoparticles using the solvothermal method in a pyridine solution, and it was followed by the removal of the CNTs. Sheng Yi and his co-workers[16] used screen printing technology and calcination to obtain an In_2O_3 NW-like network by using the CNTs templates. According to these studies, CNTs, as removable templates, play a critical role in the preparation quasi-1D metal oxide. However, many organic reagents are necessary for the method, which restricts the practical applications of the CNTs

templates. In addition, many strategies have been developed to enhance the gas sensing properties. One of the most simple and effective methods is to incorporate noble metals into the In_2O_3 structure, such as Ag,[23] Au,[24] Ru,[25] Pt[26] and Pd. In particular, palladium (Pd) has been widely applied in order to enhance the sensitivity and to shorten the response/recovery time of gas sensors.[27-31]

Pd-loaded In_2O_3 may improve the sensing performance theoretically. Kim et. al.[32] fabricated Pd-functionalized networked In_2O_3 nanowires by depositing Pd layers using a sputtering method on bare In_2O_3 nanowires. Tian et. al.[16] synthesized In_2O_3 nanowire-like network by sacrificial CNTs templates using screen printing technology and following by calcination, which need large scale of organic reagents to address the surface of CNTs. Here, we report a novel approach in order to synthesize a Pd-loaded In_2O_3 NW-like network. This was conducted by electroless plating using CNTs as templates in combination with subsequent calcination. During the procedure, Pd was introduced to activate the surface of the CNTs for the subsequent plating of indium. Moreover, following the calcination of the CNTs, which were coated with indium, the CNTs were oxidized into CO_2. This was accompanied by the transformation of metal indium into indium oxide, Additionally, Pd was in-site loaded onto In_2O_3. The response and recovery time of the gas sensor would be shortened as a result of the spillover mechanism. This approach can be applied in order to synthesize other MOS NW-like networks by plating different metals onto CNTs.

Experimental

Materials

Carboxylic multi-walled carbon nanotubes used in this work were supplied from Nanjing xfnano Technology Co. Ltd. The other chemical reagents, Stannous chloride hydrate ($SnCl_2\,2H_2O$), Palladium chloride ($PdCl_2$), hydrochloric acid (HCl), indium chloride hydrate ($InCl_3\,4H_2O$), sodium borohydride ($NaBH_4$), and absolute ethanol (C_2H_5OH), were purchased from Tianjin east Reagent Factory. All of materials were of analytical grade and used without further purification.

Preparation of the Pd-In_2O_3 NW-like network

The complicated network is comprised of quantities of NW-like structures, which are interlaced and connected with each other. The detailed formation of an individual In_2O_3 NW-like structure is schematically illustrated in Figure 1. The procedure is as follows: (1) carboxylic-MWCNTs were treated by sensitization and activation; (2) the complex of $InCl_3$ and citric acid was added into the solution of the Pd-modified CNTs; (3) $NaBH_4$ aqueous solution was slowly dropped into the mixed solution mentioned above to reduce the In^{3+} ions into In on the surface of the CNTs; (4) the CNTs coated by Pd-In were oxidized in a drying oven. (5) the Pd-In_2O_3 NW-like network structures were obtained by calcination as a result of the collapse of the CNTs and the crystallization of In_2O_3. Each concrete step of as-synthesized Pd-In_2O_3 NW-like network was shown as follow.

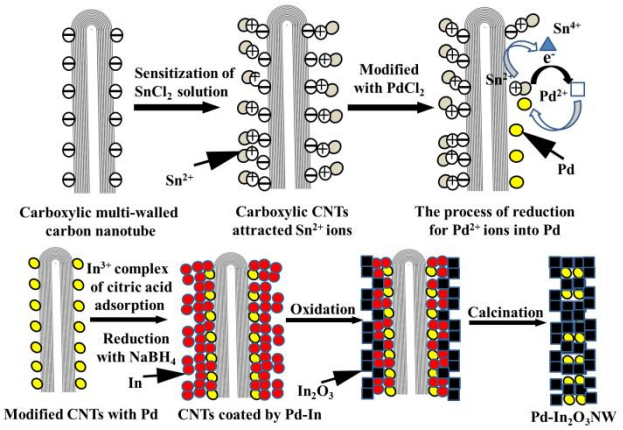

Figure 1. Schematic diagram for the preparation process of the individual NW-like In_2O_3.

A typical procedure to prepare modified CNTs with Pd consists of two steps. First step is sensitization. 0.25 g $SnCl_2{\cdot}2H_2O$ was dissolved in 25 ml 0.5 M HCl solution followed by a stirring at room temperature using a magnetic stirrer. And then 3 mg CNTs were added into the solution. After being sonicated for 15 min, the excess $SnCl_2$ was removed by washing with deionized water. Subsequently, The sensitized CNTs were immerged in 50 ml aqueous mixture of 2.5 mg $PdCl_2$ and 0.1 M HCl for activation at ambient temperature for another 15 min. then the Pd modified CNTs were washed several times with water, collected by natural sedimentation after 5 min standing. The collected CNTs mixture was dried at 90 °C for 6 h.

The modified CNTs were put into 50 ml water with 0.2 g $InCl_3$ and 0.1 g citric acid, which was sonicated for 0.5 h. At the same time, 0.3 g $NaBH_4$ was dissolved in 30 mL DI water by magnetic stirring for 10 min. Then, the $NaBH_4$ aqueous solution was slowly dropped into the above-mentioned solution at 40 °C. After 30 min, the resulting black solid products were centrifuged, washed with distilled water and ethanol to remove the ions possibly remaining in the final products, and dry at 90 °C for 60 h in air. During the period, the surface of metallic indium was oxidized into trivalent indium. Finally, the grayish yellow solid products were obtained after calcination at 550 °C for 2 h in air ambient.

Material Characterization

The crystalline phase in the samples were characterized by an X-ray diffraction (XRD, RIGAKU/ DMAX) with CuKa1 radiation (λ=0.15406nm) at a scanning rate of 2^o at 2θ min^{-1} ranging from 10^o to 90^o. The Raman spectroscopy measurement was effectuated on a Thermo Scientific DXR Raman microscope with a 532 nm laser. The BET surface area measurements were performed by nitrogen adsorption on a Quantachrome NOVA 2000 surface analyzer. XPS analysis was performed using a PHL1600ESCA instrument equipped

with an onochromatic Mg Ka X-ray source. EDS analysis was performed using X-Max80 (Oxford, UK). The surface morphologies and structures of samples were investigated by field emission scanning electron microscopy (FE-SEM, Hitachi S-4800) and transmission electron microscopy (TEM, Philips Tecnai G2 F20).

Gas sensing measurements and fabrication of gas sensors

The sensor testing system NS-4003 series (Zhong-Ke Micro-nano IOT (Internet of Things) Ltd, China) was used to evaluate the gas-sensing performance. The basic fabricated process for the fabrication of a typical Pd-In_2O_3 based gas sensor is as follow. The as-prepared Pd-In_2O_3 powder was slightly ground with absolute ethanol in an agate mortar to form a gas sensing paste. The sensor was fabricated by directly coating the paste onto the ceramic tube with four Pt wires covered on a pair of Au electrodes， A Ni–Cr alloy coil was inserted into the ceramic tube as a heater to control the operating temperature. The sensors were dried at 60 ℃ and aging at 250 ℃ for 12 h. Gas sensing test was operated in the glass test chamber, and the volume of the test chamber is 10 L. The gas concentration was adjusted by changing the amount of target gases. The response of sensor to target gas was defined as Response = R_{gas}/R_{air}, where R_{gas} and R_{air} are the resistance values of the sensor measured the in target gas and air, respectively. The response time was defined as the time required for the variation in resistance to reach 90% of the equilibrium value after a target gas was introduced, and the recovery time is the time necessary for a sensor to attain a resistance 10% above its original value when the target gas was replaced by air.

Results and discussion

The morphology of the pure CNTs was observed in TEM images, which are shown in Figure 2 a,b. It could be clearly seen that the CNTs with outer diameters (OD) of about 18 nm have a relatively smooth surface without any secondary nanostructures. After sensitization and activation, the uniformly dispersed nanoparticles attach on the surface of CNTs shown in Figure 2c. Figure 2d is a typical HRTEM image of an individual modified CNT. There are lots of dispersed Pd nanoparticles on the surface of the CNTs. These particles act as catalysts in the reaction of indium reduction,[33, 34] which makes the rate of indium deposition upon the CNTs surface much faster than that in solution. In other words, indium will be deposited preferentially on the CNTs rather than in solution. Once the metallic indium deposition was initiated, the deposited indium will act as a self-catalyst for further deposition [35].

Figure 3a (FE-SEM image) shows the general morphology characterization of the palladium modified CNTs which were coated by indium (Pd-In/CNTs) via electroless plating. It can be observed that the surfaces of the produces are obviously coarser than that of the pure CNTs. The CNTs which were coated by an indium interlace, formed a specific porous network structure. The morphology of the products was further characterized by TEM (Figure 3b).It can be observed that the modified CNTs are coated by a continuous layer with a bumpy surface. The HRTEM image (shown in the inset of Figure 3b) demonstrates that the coating layer is amorphous with an approximate size of 4 nm.

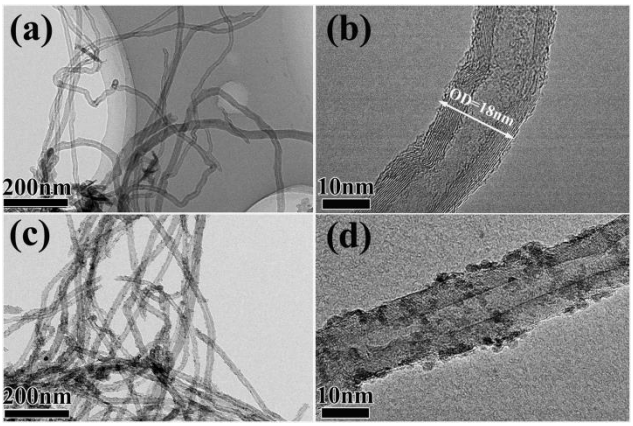

Figure 2. (a) TEM image and (b) HRTEM image of pure CNTs, (c-d) the images of morphological and compositional characterization of modified CNTs with Pd by sensitization and activation: (c) TEM image and (d) HRTEM image of an individual modified CNT.

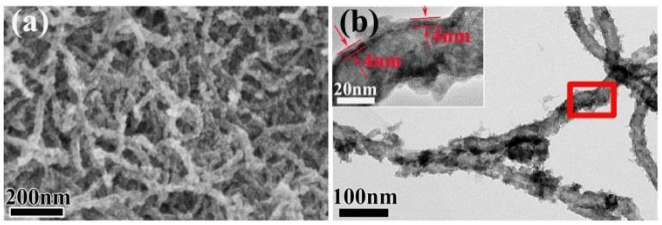

Figure 3. Morphological characterizations of Pd-In/CNTs: (a) SEM image, (b) TEM image, inset in Figure 3b is HRTEM image.

Subsequently, the Pd-In/CNTs were oxidized in air at a temperature of 90 °C. The Raman spectroscopy (Figure 4a) indicates that the pure MWCNTs mainly exhibit D, G, and G※peaks. As the oxidation time increased from 20 to 60 h, with the exception of D, G, and G※ peaks, other Raman signals appear between 200 and 650 cm^{-1}. Particularly at 60 h, five Raman scattering peaks located at 130, 304, 360, 490, and 628 cm^{-1} can be clearly observed.[36] They correlate to the reference of In_2O_3. Within the X-ray diffraction patterns (Figure 4b), the diffractions can all be readily indexed to metallic In (JCPDS 85-1409) except for the peaks at 2θ=30.6° and 26.4°. These two peaks can be indexed to the (2 1 1) crystal plane of In_2O_3 (JCPDS 71-2194) and the (0 0 2) plane of the CNTs, respectively. No peak arising from SnO_2 or PdOx/Pd can be detected because of their low content and small grain size. By calculating the areas under the In (1 0 1) and In2O3 (0 0 2) peaks for the samples which were oxidized for 20, 40, and 60 h at a temperature of 90 ℃, it can be speculated that an increase in the oxidation time leads to a gradual increase of the crystallinity of In and In_2O_3. This indicates that amorphous In can crystallize at 90 ℃, and that In was only partially oxidized into In_2O_3. Specifically, the layer coated onto the

CNTs is mainly of metallic In, even though the Pd-In/CNTs were oxidized for 60 h. The possible reason for the above phenomenon is that the metallic In would be oxidized slowly in air at 90 °C, and thus form a layer of ultrathin oxidation film, which would prevent the further oxidation of In.

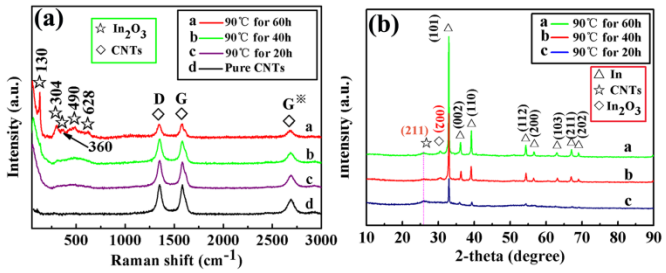

Figure 4. (a) Raman spectra, and (b) XRD patterns of Pd-In/CNTs treated for different oxidation time.

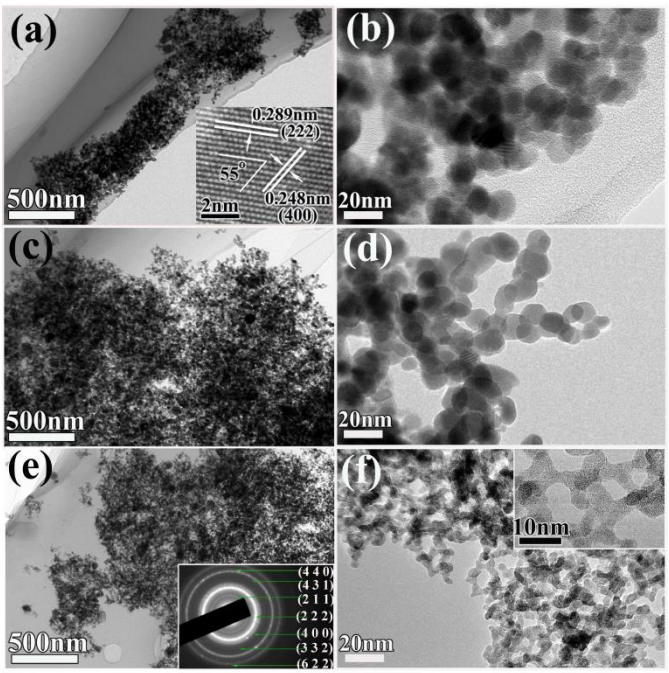

Figure 5. TEM images of morphological and compositional characterization of as-obtained Pd-In_2O_3 nanostructures by the oxidization of Pd-In/CNT for different time: (a-b) 20 h, (c-d) 40 h and (e-f) 60 h, then followed by calcination at 550 °C in air for 2 h.

In order to obtain Pd-In_2O_3 NW-like network, the CNTs should be removed. Bian, Z[37] and his coworkers reported that CNTs could be completely oxidized at 500 °C within an air atmosphere. In this study, calcination was conducted at a temperature of 550 °C for 2 h in order to remove the CNTs. Figure 5 demonstrates the morphologies of obtained Pd-In_2O_3 samples which had various oxidation times (20, 40, and 60 h). It can be observed that as the oxidation time attained to 40 h (Figure 5c,d), or 60 h (Figure 5e,f), the as-fabricated Pd-In_2O_3 replicate the structure of the CNTs, resulting in the formation of a porous NW-like network. In comparison with Figure 5d, Figure 5f exhibits a smaller grain size and more porosity. As shown in Figure 5a, b, at an oxidation time of 20 h, the Pd-In_2O_3 also replicates the structure of the CNTs. However, this Pd-In_2O_3 structure comprised of uniform nanoparticles with a size of 20 nm. As a result of the growth of the nanoparticles, it exhibited a porous structure rather than a porous NW-like network. So the as-obtained product was defined as porous Pd-In_2O_3. Furthermore, as the oxidation time increased from 20 to 60 h, the average size of the nanoparticles clearly decreased. We can clearly observed well-defined lattice fringes in the Figure 5a and the fringe spacings are approximately 0.289 and 0.248 nm, which correspond to (2 2 2) and (4 0 0) crystal planes of cubic In_2O_3. In the inset of Figure 5e, the image of the diffraction rings demonstrates that the products in this study composed of In_2O_3. The morphology of the Pd-In_2O_3 NW-like network was further observed in Figure 5f, which clearly shows that a large quantity of extremely thin NW-like In_2O_3 was interwoven into a porous network. Moreover, within the inset of Figure 5f, some individual NW-like In_2O_3 with a diameter of 8 nm can be clearly observed. There are many pores among the network. The pores will significantly improve the properties of gas sensors because of their larger surface-to-volume ratios and because there are more channels for gas diffusion.[16, 38] To conclude, the oxidation time for 60 h was chosen to prepare Pd-In_2O_3 NW-like network.

It should be noticed that the morphologies of In_2O_3 changed from near-spherical nanoparticles into irregular nanoparticles. This may be because metallic In has rapid diffusion rate when temperature exceeds its melting point. Owing to the surface tension, molten In tends to form a near-spherical structure in order to achieve lowest surface free energy. However, as shown in the above Raman spectra and XRD patterns, the amount of In_2O_3 increases with the oxidation time. Therefore, we proposed a possible reason for the formation of the NW-like structure. First, a layer of In_2O_3 film is formed onto the In surface at a temperature of 90 °C (in air), and subsequently, the thickness of the In_2O_3 film increases with the oxidation time. At an oxidation time of 60 h, the In_2O_3 film is thick enough to restrict the flow of molten indium and the diffusion at high temperature. Thus, the size and structure of the metallic In is maintained. Subsequently, the internal In is further oxidized into In_2O_3, This is accompanied by the collapse of the CNTs and the contraction of In_2O_3, forming an individual NW-like In_2O_3 structure. It reveals oxidation time plays an important role in the synthesis of the Pd-In_2O_3 NW-like network.

To determine the existence of the Pd element in the as-obtained Pd-In_2O_3 NW-like network, EDS analysis was carried out. Figure 6 shows the EDS analysis of the obtained Pd-In_2O_3. The EDS spectrum shown in Figure 6a indicates that the composite consists of In, O and Pd. Moreover, a trace of Sn element was observed due to the sensitization of $SnCl_2$. The carbon and Cu peaks are attributed to the copper–carbon grid. One point should be emphasized that the effects of Sn element will not be considered in the following performance testing because all the samples were sensitized by the same sensitization condition. EDS elemental map of In, O, and Pd elements are shown in Figure 6c–e, respectively. The recorded images of In and O mapping are contributed to In_2O_3. Besides that,

the elemental map of Pd corresponding with STEM image shown in Figure 6b indicates that Pd element is uniformly distributed into In_2O_3. In addition, the state of Pd in Pd-In_2O_3 NW-like network was investigated by XPS analysis as shown in Figure S1. It reveals that palladium has been partially oxidized at 550 °C, forming PdO and PdOx/Pd. Therefore, only part of Pd among them can enhance the gas sensing properties.

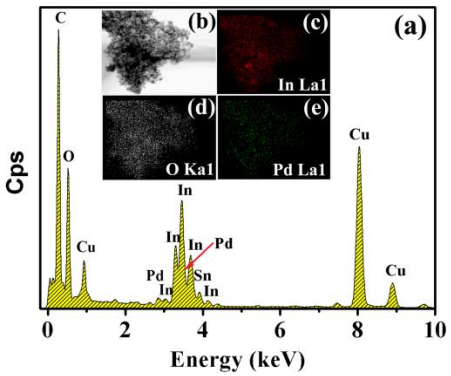

Figure 6. (a) EDS analysis spectrum and (b) STEM image of Pd-In_2O_3 NW-like network, (c-e) EDS mapping of In, O and Pd elements.

The porous unloaded In_2O_3 was produced by the same method as that of the porous Pd-In_2O_3, except for the absence of $PdCl_2$ (displayed in Figure S2). It is noteworthy that the morphology and grain size of the porous unloaded In_2O_3 is essentially the same as that of the porous Pd-In_2O_3. Its precursor (In/CNTs) was also observed using a TEM, as shown in Figure S3. It indicates Pd also plays a significant role in the preparation of the Pd-In_2O_3 NW-like network.

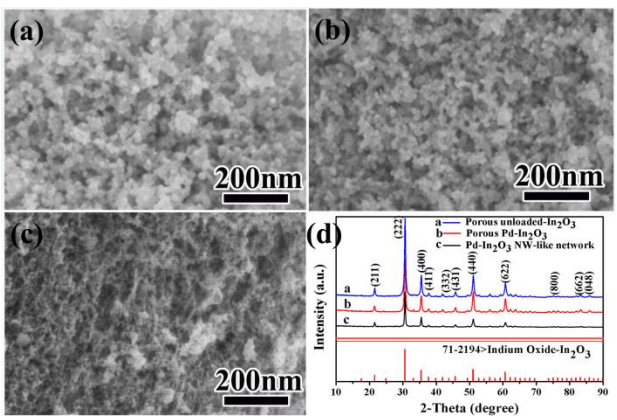

Figure 7. SEM images of (a) porous unloaded-In_2O_3, (b) porous Pd-In_2O_3, (c) Pd-In_2O_3 NW-like network and (d) XRD patterns of as-obtained In_2O_3 samples applied in Gas sensing properties.

In order to facilitate subsequent measurement of gas sensing, SEM images of as-obtained porous unloaded-In_2O_3, porous Pd-In_2O_3, and Pd-In_2O_3 NW-like network were shown in Figure 7a-c and XRD patterns were merged in Figure 7d. All the reflections in the pattern are well assigned to a pure cubic In_2O_3 (JCPDS 71-2194) without peaks arising from other phases such as PdOx/Pd and SnO_2. The peak intensity of porous Pd-In_2O_3 and porous unloaded-In_2O_3 are comparable but higher than that of Pd-In_2O_3 NW-like network. It may be affected by the grain size and crystallinity of the obtained products, which are in accordance with the HRTEM results.

To understand the gas sensing properties and mechanism of as–obtained Pd-In_2O_3 NW-like network, gas sensing measurements were carried out. For comparison, the sensing performances of the as-prepared porous unloaded-In_2O_3 and porous Pd-In_2O_3 were also studied. Figure 8a shows the response curves of three samples at different operating temperatures under exposure to 5 ppm NO_2. Obviously, the responses of all tested sensors varying with operating temperature are in a similar tendency, which increases with temperature firstly, up to their maximum at 110 °C, and then decreased rapidly with operating temperature further increasing. In addition, the maximum response of Pd-In_2O_3 NW-like network sensor can reach 27, which is about 5 times larger than that of porous unloaded-In_2O_3 and porous Pd-In_2O_3 (their response values are about 6.2 and 5.5, respectively). As a consequence, the optimized 110 °C was chosen for further gas sensing analysis. Figure S4 displays the response of three sensors with NO_2 concentrations ranging from 1 to 20 ppm at 110 °C. Similarly, the Pd-In_2O_3 NW-like network sensor presented much higher response than that of the other two sensors. It is attributed to the higher surface to volume ratio and more channels for gas diffusion. In addition, the two sensors with the similar morphology but different components have the same response value at various concentrations of NO_2. The BET surface areas of three sensors (porous unloaded-In_2O_3, porous Pd-In_2O_3, and Pd-In_2O_3 NW-like network) calculated from 5-point BET surface area plots (Figure S5) are about 548.200, 550.101, 1327.035 m^2/g, respectively, indicating that NW-like network sensor presents much higher surface to volume ratio than that of the other two sensors.

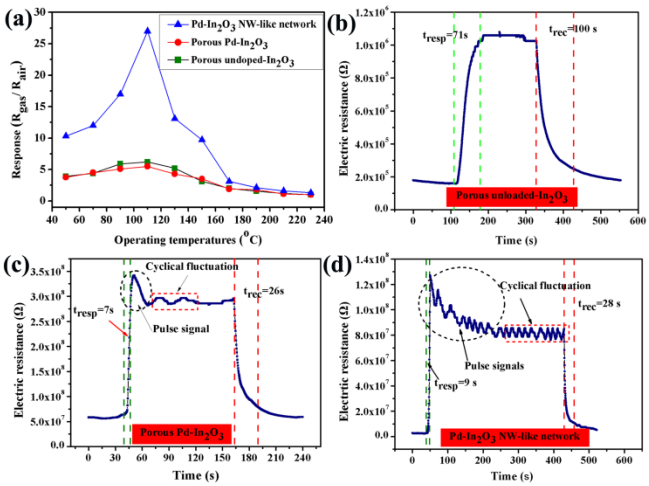

Figure 8. (a) Dependence of the gas sensor response at various operating temperatures of as- obtained samples toward 5 ppm NO_2. Dynamic response curves of (b) porous unloaded-In_2O_3, (c) Pd-In_2O_3, (d) Pd-In_2O_3 NW-like network sensors at optimum operating temperature (110 °C).

Figure 8b-d shows the dynamic response curves of the three In_2O_3-based sensors towards 5 ppm NO_2 at a temperature of 110 °C. It can be observed that the electric resistance of the sensors increased abruptly on exposed to NO_2, and subsequently decreased to its initial value following the release of NO_2. The response and recovery times of the Pd-In_2O_3 NW-like network (shown in Figure 8d) were approximately 9 and 28 s, respectively，and in Fig 8c, the corresponding values were about 7 and 26 s for the porous Pd-In_2O_3. However, the response and recovery times of the porous unloaded-In_2O_3 sensors were the longest (71 and 100 s (in Figure 8b)). This implies that the response and recovery times can be dramatically shortened by Pd loading. The curves in Figure 8c and 8d are obviously different from that shown in Figure 8b. One or more sharp prominent signals, denoted as "pulse signal", appeared once the sensors were exposed to NO_2. Moreover, as the measured time increased, the resistance of the sensors gradually decreased initially, and subsequently fluctuated around a certain equilibrium value (this value was applied in response calculation instead of R_{gas} when the "cyclical fluctuation" appeared), and finally achieved dynamic equilibrium.

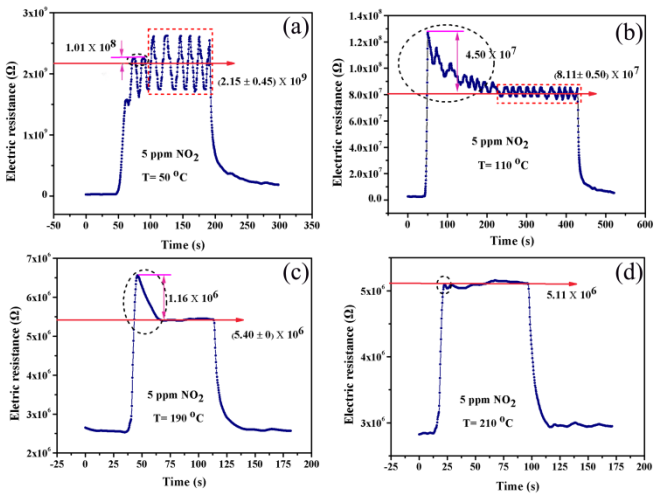

Figure 9. Typical dynamic response curves of the Pd-In_2O_3 NW-like network sensor exposed to 5 ppm NO_2 at different temperatures: (a) 50 ℃，(b) 110 ℃, (c), 190 ℃，and (d) 210 ℃.

Figure 9 clearly demonstrates the typical dynamic response curves of the Pd-In_2O_3 NW-like network sensor towards 5 ppm NO_2 at various temperatures. It can be observed that four curves possess respective characteristics. The curve shown in Figure 9a was measured at 50 °C. It demonstrates higher amplitude (approximately $0.45\times10^9\,\Omega$) than that of "pulse signal" (approximately $1.01\times10^8\,\Omega$). At 110 °C, the amplitude is only $0.50\times10^7\,\Omega$ (Figure 9b), and at an operating temperature of 190 °C, it even disappears, as shown in Figure 9c. The "Pulse signal" demonstrates the same trend. It decreases as the operating temperature increases and disappears at approximately 210 °C (Figure 9d). Moreover, the same result was obtained from the response curves of the porous Pd-In_2O_3, as shown in Figure S6. Until now, few reports on this gas sensing phenomenon were found in the literature searching. In order to prove the two novel characteristics, "pulse signal" and "cyclical fluctuations" to be reproducible, the gas sensing measurements of Pd-In_2O_3 NW-like network prepared 3 month ago were carried out. As show in Figure S7, we can see that there are almost no changes in the response curves, which confirms the good stability of the sensor.

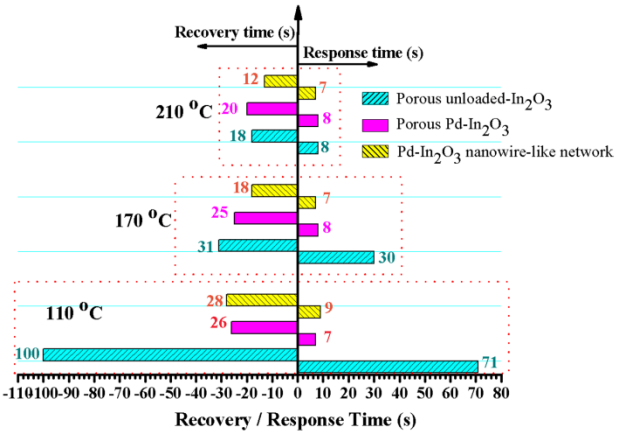

Figure 10. Histograms about response/recovery time of porous unloaded-In_2O_3, porous Pd-In_2O_3, and Pd-In_2O_3 NW-like network sensors to 5 ppm NO_2 at 110, 170 and 210 ℃.

Response/recovery time of gas sensor is also important for practical application, and their changes can provide an intuitive demonstration to understand gas sensing mechanism. Figure 10 shows the response/recovery time of three sensors exposed to 5 ppm NO_2 at different operating temperatures (110, 170 and 210 ℃). Both the response and recovery time of porous unloaded-In_2O_3 sensor dramatically shorten from 71 to 8s and 100 to 18s with the operation temperature rising. Nevertheless, there is a little variation of response/recovery time for sensors with Pd loading at various temperatures. The unloaded one presents much sensitive to temperature, which was described further in Figure S8. It proved that Pd-loaded In_2O_3 and unloaded-In_2O_3 involve two key mechanisms, namely electric effects and chemical effects.[31]

For In_2O_3-based gas sensors, the gas sensing mechanism can be explained by the changes of resistance, which is attributed to the increase or decrease of free electron concentration caused by adsorption or desorption of gas molecules on the In_2O_3 surface.[2] When the sensors were exposed to air, O_2 adsorbed on the surface and the absorbed oxygen captured electrons from the sensors to generate chemisorbed oxygen species (O_2^-, $O^-$and O^{2-}) through Eqs. (1-4). This will cause a resistance increase of the In_2O_3 sensors (R_a).[1, 7, 8]

$$O_{2(gas)} \rightarrow O_{2(ads)} \quad (1)$$

$$O_{2(ads)} + e^- \rightarrow O_{2\,(ads)}^- \quad (2)$$

$$O_{2\,(ads)}^- + e^- \rightarrow 2O_{(ads)}^- \quad (3)$$

$$O_{(ads)}^- + e^- \rightarrow O_{(ads)}^{2-} \quad (4)$$

Among In_2O_3-based gas sensors, gas sensing of porous unloaded In_2O_3 is attributed to electric effects. When the sensors were exposed

to NO_2, the adsorbed NO_2 molecules not only capture the electrons from the surface of In_2O_3, but also directly react with the chemisorbed oxygen species, forming adsorbed $NO_2^-{}_{(ads)}$, as shown by Eqs. (5-6).[39]

$$NO_{2(gas)} + e^- \rightarrow NO_2^-{}_{(ads)} \quad (5)$$

$$NO_{2(gas)} + O_2^-{}_{(ads)} + 2e^- \rightarrow NO_2^-{}_{(ads)} + 2O^-{}_{(ads)} \quad (6)$$

In the above reactions, the electrons in the In_2O_3 are transferred to $NO_{2\ (gas)}$ or the $O^-{}_{2\ (ads)}$. The process leads to the increase of the resistance due to the decrease of the electron concentration in the In_2O_3. Actually, it is difficult to capture electrons from In_2O_3, because reactive energy barrier cannot be overcome at low temperature.

However, for Pd-loaded In_2O_3, Pd as a catalyst generally plays an important role in enhancing the response/recovery time. It dramatically activates the dissociation of oxygen molecules on the surface of sensors and makes the adsorbed oxygen species increasing.[28, 31] Simultaneously, NO_2 is a very efficient source of oxygen adatoms due to the catalyzation of Pd. When NO_2 was introduced, NO_2 molecules are partially decomposed into adsorbed NO (NO_{ads}) and oxygen adatoms on the surface of Pd (O_{ads}(Pd)) through Eq. (7). Moreover, the dissociated oxygen atoms (O_{ads}) are transferred to In_2O_3 by means of the spillover effect and capture electrons from In_2O_3, which leads to the increase of the resistance in NO_2, as shown by Eqs. (8-9).[32]

$$NO_{2(gas)} + Pd \rightarrow NO_{ads} + O_{ads}(Pd) \quad (7)$$

$$O_{ads}(Pd) + In_2O_3 \rightarrow O_{ads}\,(In_2O_3) \quad (8)$$

$$O_{ads}\,(In_2O_3) + e^- \rightarrow O^-{}_{ads}\,(In_2O_3) \quad (9)$$

$$O^-{}_{ads}\,(In_2O_3) + NO_{ads} \rightarrow NO_2 + e^- \quad (10)$$

O_{ads} is much more active than $NO_{2(gas)}$ and $O_2^-{}_{(ads)}$, so the rate of capturing electrons happened in Eq. (9) is faster than that in Eqs. (5-6). Thus, Pd loaded In_2O_3 sensors possess shorter response/ recovery time. Meanwhile, adsorbed NO will be oxidized into NO_2 on the surface of Pd-In_2O_3 sensors and release electrons into In_2O_3, leading to the decrease of the resistance [40], as shown by Eq. (10). These chemical equations and the chemical effects can be used to explain the appearance of above response curves.

According to the spillover mechanism, the loading of Pd onto In_2O_3 can dramatically increase the chemisorption of NO_2. After exposed to NO_2, the Pd-In_2O_3 sensors dissociate NO_2 into NO and O^-. This is rapidly accompanied by the capturing of electrons from the In_2O_3 surface. Thus, the resistance of the sensor increases to a maximum value within a short time. Subsequently, the dissociated NO will react with the chemisorbed oxygen species. According to the Eq. (10), the electrons trapped by the dissociated oxygen species are released and then re-injected into the In_2O_3, which decreases the resistance of the sensor. So the resistance of sensor falls down after it ascends first, and finally tends to be equilibrium, thus forming the "pulse signal". As the time increases, the NO_2 dissociation and the NO adsorption reach dynamic equilibrium. But the two reactions are asynchronous. Firstly, the NO_2 dissociation was dominant. It increased the resistance. Then, the reaction between NO and the adsorption oxygen species occurred along with the resistant decrease, when the NO concentrations reached a certain state. Contrastingly, as the NO was consumed to a low concentration, the NO_2 dissociation was predominant again. These two asynchronous reactions repeated until equilibrium conditions exist, contributing to the appearance of the "cyclical fluctuations". It is noteworthy that loading of Pd always enhances the response of the gas sensor. In this study, the response of the porous Pd-In_2O_3 is the same as that of the porous In_2O_3 without Pd loading. Introducing Pd into In_2O_3 did not improve the response of In_2O_3. The possible reason is as follows: On the one hand, when NO_2 was introduced, Pd catalyzed the decomposition of NO_2 through Eq. (7), and the dissociated oxygen atoms (O_{ads}) captured electrons from In_2O_3, resulting in the increase of the resistance in NO_2 (marked by $R_{gas}\uparrow$). On the other hand, loading of Pd dramatically activated the dissociation of oxygen (in air) on the surface of sensor. Because more electrons were captured by oxygen molecules, the R_{air} (the resistance of the intrinsic In_2O_3) increased (marked by $R_{air}\uparrow$). Therefore, the catalysis of Pd not only increased the R_{gas}, but also promoted the R_{air}. In conclusion, Response ($R=R_{gas}\uparrow/R_{air}\uparrow$) of the porous Pd-$In_2O_3$ was not enhanced.

The correlation of the "pulse signal" and the "cyclical fluctuations" with the operating temperature in the response curve of the Pd-In_2O_3 NW-like network sensor can be explained by the synergy of the chemical and electric effects. At a low temperature (50 ℃), the adsorbed gas (NO) molecules are not sufficiently activated to overcome the activation energy barrier to react with the adsorption oxygen species.[7] The reaction between NO and the adsorption oxygen species difficultly occur until enough NO_2 is dissociated, which induces a high amplitude of pulse and fluctuation. As a temperature of 110 ℃, the operating temperature is at an optimum for chemical effects to occur. But the reaction rates between NO and the adsorption oxygen species increase more rapidly than that of the NO_2 decomposition. It induces the decrease of fluctuation amplitude.[41] Subsequently, the reaction in the Eq. (10) accelerates at a higher temperature (such as 190 ℃), causing the generated NO to be absorbed rapidly and oxidized without delay. Therefore, the "cyclical fluctuation" disappears. As the temperature increases, the reaction between NO and the adsorption oxygen species almost ceases as a result of insufficient compensation for the increased surface reactivity. This is a possible reason for the disappearance of "pulse signal".

Conclusions

In summary, a Pd-loaded In_2O_3 NW-like network was first synthesized via electroless plating using CNTs as templates in combination with subsequent oxidation and calcination. The preparation process was studied and it was determined that the morphology of samples can be controlled by oxidation time. The activation of palladium (Pd) played important roles in replicating the structure of the CNTs in order to form a NW-like network. Gas

sensing measurements revealed the response of Pd-loaded In_2O_3 NW-like network was 27, which was approximately 5 times greater than that of the porous Pd-In_2O_3 (approximately 5.5) when exposed to NO_2 concentrations as low as 5 ppm at a temperature of 110 ℃. In addition, results showed that Pd loading is an effective approach to shorten the response and recovery times. On exposure to NO_2 at a concentration of 5 ppm at a temperature of 110 ℃, the response and recovery times of the Pd-In_2O_3 NW-like network were approximately 9 and 28 s, respectively. For the porous unloaded-In_2O_3, the corresponding values were approximately 71 and 100 s. Moreover, two novel characteristics were discovered: the "pulse signal" and "cyclical fluctuations". This has the potential to be applied to the preparation of multi-functional gas sensors, and for the quantitative detections. Finally, the synergy of the chemical and electric effects was introduced to explain these results. Our results and findings suggest that the Pd-In_2O_3 NW-like network is a promising candidate to monitor and control NO_2 in terms of its low detection limit, high response, and short response/recovery time.

Acknowledgements

Financial support by National Natural Science Foundation of China (51402211) is gratefully acknowledged.

Notes and references

[a] School of Materials Science and Engineering, Tianjin University, Tianjin 300072, China
[b] Tianjin Key Laboratory of Composite and Functional Materials, Tianjin 300072, China
*Corresponding author. Tel: +86 22 27402494
E-Mail: yqliang@tju.edu.cn
Electronic Supplementary Information (ESI) available: Figure S1-S8.
See DOI: 10.1039/b000000x/

References

1 P. Li, H. Fan, Y. Cai and M. Xu, *CrystEngComm*, 2014, **16**, 2715-2722.
2 C. Zhao, G. Zhang, W. Han, J. Fu, Y. He, Z. Zhang and E. Xie, *CrystEngComm*, 2013, **15**, 6491-6497.
3 J. Zai, J. Zhu, R. Qi and X. Qian, *J. Mater. Chem. A*, 2013, **1**, 735-745.
4 Y. F. Sun, S. B. Liu, F. L. Meng, J. Y. Liu, Z. Jin, L. T. Kong and J. H. Liu, *Sensors (Basel)*, 2012, **12**, 2610-2631.
5 N. Siedl, P. Gugel and O. Diwald, *Langmuir*, 2013, **29**, 6077-6083.
6 F. Gu, L. Zhang, Z. Wang, D. Han and G. Guo, *Sens. Actuators B: Chem.*, 2014, **193**, 669-678.
7 P. Song, D. Han, H. H. Zhang, J. Li, Z. X. Yang and Q. Wang, *Sens. Actuator B: Chem.*, 2014, **196**, 434-439.
8 S. Elouali, L. G. Bloor, R. Binions, I. P. Parkin, C. J. Carmalt and J. A. Darr, *Langmuir*, 2012, **28**, 1879-1885.
9 N. Singh, R. K. Gupta and P. S. Lee, *ACS Appl. Mater. Interfaces*, 2011, **3**, 2246-2252.
10 J. Liu, W. Li, L. H. Zhu, C. Li, F. D. Qu, W. B. Guo, C. H. Feng and S. P. Ruan, *J. Nanosci. Nanotechnol.*, 2014, **14**, 3653-3657.
11 X. Lu and L. Yin, *J. Mater. Sci. Technol.*, 2011, **27**, 680-684.
12 Y. Li, J. Xu, J. Chao, D. Chen, S. Ouyang, J. Ye and G. Shen, *J. Mater. Chem.*, 2011, **21**, 12852-12857.
13 W. J. Tseng, T. T. Tseng, H. M. Wu, Y. C. Her, T. J. Yang and P. Gouma, *J. Am. Chem. Soc.*, 2013, **96**, 719-725.
14 N. Du, H. Zhang, X. Ma and D. Yang, *Chem. Commun. (Camb.)*, 2008, 6182-6184.
15 Z. Zanolli, R. Leghrib, A. Felten, J. J. Pireaux, E. Llobet and J. C. Charlier, *Acs Nano*, 2011, **5**, 4592-4599.
16 S. Yi, S. Tian, D. Zeng, K. Xu, S. Zhang and C. Xie, *Sens. Actuators B: Chem.*, 2013, **185**, 345-353.
17 A. Gurlo, *Nanoscale*, 2011, **3**, 154-165.
18 L. Xu, B. Dong, Y. Wang, X. Bai, Q. Liu and H. Song, *Sens. Actuators B: Chem.*, 2010, **147**, 531-538.
19 S. K. Lim, S. H. Hwang, D. Chang and S. Kim, *Sens. Actuators, B: Chem.*, 2010, **149**, 28-33.
20 W. Zheng, X. Lu, W. Wang, Z. Li, H. Zhang, Y. Wang, Z. Wang and C. Wang, *Sens. Actuators B: Chem.*, 2009, **142**, 61-65.
21 N. Du, H. Zhang, B. D. Chen, X. Y. Ma, Z. H. Liu, J. B. Wu and D. R. Yang, *Adv. Mater.*, 2007, **19**, 1641-1645.
22 D. Zhang, C. Pan, L. Shi, L. Huang, J. Fang and H. Fu, *Microporous Mesoporous Mat.*, 2009, **117**, 193-200.
23 Y. Zhang, Z. Zheng and F. Yang, *Ind. Eng. Chem. Res.*, **49**, 3539-3543.
24 C. K. Tagad, K. S. Rajdeo, A. Kulkarni, P. More, R. C. Aiyer, S. Sabharwal, *RSC Adv.*, 2014, **4**, 24014.
25 Z. Zhu, R. C. Deka, A. Chutia, R. Sahnoun, H. Tsuboi, M. Koyama, N. Hatakeyama, A. Endou, H. Takaba, C. A. Del Carpio, M. Kubo and A. Miyamoto, *J. Phys. Chem. Solids*, 2009, **70**, 1248-1255.
26 Zuruzi, M. H. Nurmawati, Y. H. Yeo, S. X. Wu, P. C. H. Lai, Z. Chen, *RSC Adv.*, 2013, **3**, 19971.
27 Y. Sun and H. H. Wang, *Adv. Mater.*, 2007, **19**, 2818-2823.
28 C. Liewhiran, N. Tamaekong, A. Wisitsoraat, A. Tuantranont and S. Phanichphant, *Sens. Actuators B: Chem.*, 2013, **176**, 893-905.
29 S. J. Pearton, F. Ren, Y.-L. Wang, B. H. Chu, K. H. Chen, C. Y. Chang, W. Lim, J. Lin and D. P. Norton, *Prog. Mater Sci.*, 2010, **55**, 1-59.
30 A. Shanmugasundaram, B. Ramireddy, P. Basak, S. V. Manorama and S. Srinath, *J. Phys. Chem. C*, 2014, **118**, 6909-6921.
31 H. Y. Lai and C. H. Chen, *J. Mater. Chem.*, 2012, **22**, 13204-13208.
32 S. S. Kim, J. Y. Park, S.-W. Choi, H. G. Na, J. C. Yang and H. W. Kim, *J. Alloys Compd.*, 2011, **509**, 9171-9177.
33 J. Sittikun, Y. Boonyongmaneerat, P. Weerachawanasak, P. Praserthdam and J. Panpranot, *Reac. Kinet. Mech. Cat.*, 2014, **111**, 123-135.
34 L. S. Zhong, J. S. Hu, Z.-M. Cui, L. J. Wan and W. G. Song, *Chem. Mater.*, 2007, **19**, 4557-4562.
35 L. M. Ang, T. S. A. Hor, G. Q. Xu, C. H. Tung, S. P. Zhao and J. L. S. Wang, *Carbon*, 2000, **38**, 363-372.
36 L. N. Jin, Q. Liu and W. Y. Sun, *CrystEngComm*, 2013, **15**, 4779-4784.
37 Z. Bian, J. Zhu, F. Cao, Y. Huo, Y. Lu and H. Li, *Chem. Commun.*, 2010, **46**, 8451-8453.
38 E. Comini, C. Baratto, G. Faglia, M. Ferroni, A. Vomiero and G. Sberveglieri, *Prog. Mater Sci.*, 2009, **54**, 1-67.
39 J. Zhao, T. Yang, Y. Liu, Z. Wang, X. Li, Y. Sun, Y. Du, Y. Li and G. Lu, *Sens. Actuators B: Chem.*, 2014, **191**, 806-812.
40 B. M. Weiss and E. Iglesia, *J. Catal.*, 2010, **272**, 74-81.
41 C. S. Rout, K. Ganesh, A. Govindaraj and C. N. R. Rao, *Appl. Phys. A*, 2006, **85**, 241-246.

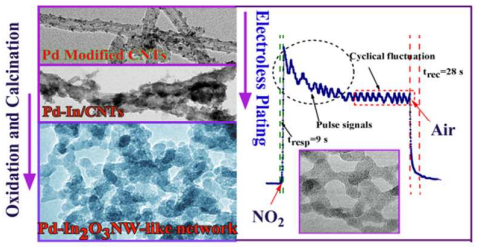

TOC

Pd-In_2O_3 NW-like network sensor with characteristic response curve has a potential application in preparing multi-functional gas sensors.